Experimental Evidence of Cubic Rashba Effect in an Inversion-Symmetric Oxide

H. Nakamura,[1,3] T. Koga,[2] and T. Kimura[1]

[1]*Division of Materials Physics, Graduate School of Engineering Science, Osaka University, Toyonaka, Osaka 560-8531, Japan*
[2]*Division of Electronics for Informatics, Graduate School of Information Science and Technology, Hokkaido University, Hokkaido 060-0814, Japan*
[3]*PRESTO, Japan Science and Technology Agency (JST), Saitama 332-0012, Japan*

(Received 19 December 2011; published 14 May 2012)

We present evidence of cubic Rashba spin splitting in a quasi-two-dimensional electron gas formed at a surface of (001) $SrTiO_3$ single crystal from the weak localization or antilocalization (WAL) analysis of the low-temperature magnetoresistance. Our WAL data were well fitted by the model assuming $m_j = \pm 3/2$ for the spin-split pair, in which 2π rotation of the electron wave vector $\mathbf{k}_\parallel$ in the k_x-k_y plane accompanies 6π rotation of the spin quantization axis. This finding pertains to the p symmetry of the t_{2g} electronic band derived from d electrons in $SrTiO_3$, which provides insights into the surface electronic state of (001) $SrTiO_3$.

DOI: 10.1103/PhysRevLett.108.206601 PACS numbers: 72.25.Dc, 72.25.Rb, 73.20.Fz, 73.61.Le

The Rashba effect is a manifestation of spin-orbit interaction (SOI) in solids, where spin degeneracy associated with the spatial inversion symmetry is lifted due to a symmetry-breaking electric field normal to the heterointerface [1]. In general, the Hamiltonian of the spin-orbit interaction is given by $(\nabla V \times \mathbf{p}) \cdot \boldsymbol{\sigma}$, and for the perpendicular electric field $\nabla V = (0, 0, E_z)$, results in a conventional k-linear Rashba effect, where $\boldsymbol{p}$ is an electron's momentum, and $\boldsymbol{\sigma}$ is the Pauli spin matrices. The lack of inversion symmetry in an underlying bulk also leads to a spin splitting called the Dresselhaus SOI. The nature of Rashba and Dresselhaus SOI, such as the k dependence of spin splitting energy, has been studied extensively [2–12].

The conduction band of $SrTiO_3$ originates from Ti $3d$ orbitals, which exhibit outstanding electronic properties such as an interface superconductivity and magnetism [13–16]. Because of the crystal field, three spin-degenerate t_{2g} bands (yz, zx, xy-like states) form the bottom of the conduction band [17,18]. An atomic $\boldsymbol{l} \cdot \boldsymbol{s}$-coupling causes the splitting of t_{2g} states (~ 17 meV in Ref. [19]; also see Ref. [18]). Thus, the lowest energy states for bulk $SrTiO_3$ consist of fourfold degenerate bands, which correspond to total angular momentum $J = 3/2$ ($m_j = \pm 3/2$ and $\pm 1/2$) states in atoms. Recent studies based on density-functional theory [20] and photoemission experiments [21] suggest that the quantum confinement lifts degeneracy of these bands at $\boldsymbol{k} = 0$, and that the lowest energy state has an xy-like character. The xy state has a dominant coupling to the $m_j = \pm 3/2$ state in an angular momentum basis [22].

The Rashba spin splitting in $m_j = \pm 3/2$ bands is described by the effective cubic-Rashba Hamiltonian [2,23]

$$H_{R3} = \beta E_z i (k_-^3 \sigma_+ - k_+^3 \sigma_-). \qquad (1)$$

Here, $\sigma_\pm = 1/2(\sigma_x \pm i\sigma_y)$, σ_x and σ_y denote Pauli spin matrices, $k_\pm = k_x \pm i k_y$, and k_x, k_y are the components of an in-plane wave vector $\boldsymbol{k}_\parallel$ [2,23]. A prerequisite for the spin splitting in $m_j = \pm 3/2$ bands is the off-diagonal coupling between $m_j = \pm 3/2$ and $m_j = \pm 1/2$ bands [2,23] in the scheme of envelope function approximation. This coupling is induced by an inversion breaking electric field in a quantum well or just by the presence of an interface [2,23]. For GaAs, where the cubic-Rashba effect has been studied previously [2,8,9,23], the bulk inversion asymmetry, which causes off-diagonal terms in a Kane model, also gives rise to k-cubic spin splitting (cubic Dresselhaus term) [2]. In contrast, bulk $SrTiO_3$ is inversion symmetric and no Dresselhaus terms occur, which is a great advantage for the study of the cubic-Rashba effect. By calculating the spin expectation value using the eigenfunctions for Eq. (1) (shown explicitly in Ref. [24]), we obtain the following effective magnetic field $\boldsymbol{\Omega}_{R3}$:

$$\boldsymbol{\Omega}_{R3}(\mathbf{k}_\parallel) = |\boldsymbol{\Omega}_{R3}|(\pm \sin 3\theta, \mp \cos 3\theta), \qquad (2)$$

where θ is an angle $\mathbf{k}_\parallel$ forms with the k_x axis, and the $\pm$ signs correspond to the two spin directions. Thus, $\boldsymbol{\Omega}_{R3}$ rotates within the k plane 3 times as many times as the conventional Rashba effect in which $\boldsymbol{\Omega}_{R1}(k_\parallel) = |\boldsymbol{\Omega}_{R1}|(\pm \sin\theta, \mp \cos\theta)$ [Fig. 4(a)].

In this Letter, we study the Rashba effect in top-gated $SrTiO_3$ by weak localization or antilocalization (WAL) analysis of the magnetoresistance (MR). We report the observation of a large WAL in an electron accumulation layer of $SrTiO_3$. It is shown that the WAL data cannot be fitted by the k-linear Rashba splitting model, but can be fitted perfectly by the k^3 spin splitting model. This indicates that the spin splitting of $m_j = \pm 3/2$ bands as discussed above is indeed taking place in $SrTiO_3$. The previous reports on the successful fitting of WAL in $LaAlO_3/SrTiO_3$ interfaces [25,26] by Maekawa-Fukuyama theory [27], which assumes Elliot-Yafet spin relaxation and does not include the k-dependent Rashba terms, may be attributed to the mathematical identity [5] of the Hikami-Larkin-Nagaoka model [28] (a simpler version of Maekawa-Fukuyama theory) with the k-cubic spin splitting model [29].

Field-effect transistors (FETs) were fabricated on the (100) face of $SrTiO_3$ single crystals using parylene as a gate insulator [30]. We have adopted a bilayer (Al/Zn) source-drain contact [31] as well as a Hall-bar shaped gate contact in the present devices [Fig. 1(a)]. We have fabricated three devices with different parylene thicknesses: 0.43 μm (STO-A), 0.40 μm (STO-B), and 0.36 μm (STO-C). STO-A and -B were fabricated on as-received $SrTiO_3$ single crystals grown by a vendor (Furuuchi Corp.). For STO-C, the surface etching of the substrate was performed prior to the FET fabrication using buffered hydrofluoric acid (0.1 wt% HF). Temperature and magnetic field B were controlled by a physical property measurement system (Quantum Design). Resistivity and Hall measurements were carried out by conventional low-frequency lock-in technique (5.7–13 Hz) with a current of 0.5–1 μA.

In Figs. 1(b)–1(d), we show transport properties of $SrTiO_3$-FETs at 2 K. As seen in the sheet resistivity R_{xx} as a function of an applied electric field to the top gate E_G [Fig. 1(b)], an electron gas at the $SrTiO_3$ accumulation layer is successfully tuned by E_G. Measured sheet carrier density n_s, estimated by the Hall measurement [Fig. 1(d)], covers the range 2–8 $\times 10^{12}$ cm^{-2}, where n_s increases monotonically with E_G [Fig. 1(c)]. The corresponding Hall mobility is in the range from ~500 to ~2300 cm^2/V s and also increases monotonically with E_G.

Figure 2(a) shows a raw MR curve taken at 2 K. The experimental MR curve (open circles) shows a clear structure around $B = 0$ T, which we attribute to weak antilocalization [27,28,32]. The broader positive MR proportional to B^2 is due to the classical Lorentz force. By subtracting the B^2 background from the magnetoconductance plot and then shifting the obtained conductance difference to the origin, we obtained a weak localization or antilocalization correction to the conductivity ($\Delta\sigma$) as shown in Fig. 2(b). In the following part of the manuscript, we concentrate on $\Delta\sigma$.

The WAL data were fitted using a theoretical model devised by Iordanskii, Lyanda-Geller, and Pikus (ILP theory) [5,32]. The theory incorporates k-dependent spin-precession vector $\mathbf{\Omega}_1(\mathbf{k}_\parallel) = |\mathbf{\Omega}_1|(\sin\theta, -\cos\theta)$ and $\mathbf{\Omega}_3(k_\parallel) = |\mathbf{\Omega}_3|(\sin 3\theta, -\cos 3\theta)$ [33]. The theory is applicable to a diffusive regime, i.e., $B < B_{\mathrm{tr}} = \hbar/2el_m^2$, where B_{tr} is the transport field characterizing elastic scattering of electrons, $\hbar$ is the Planck's constant divided by 2π, e is the electron charge, and l_m is the mean free path. We thus limited our fitting to $B < B_{\mathrm{tr}}$ (B_{tr} ranged from 0.05 to 1.8 T

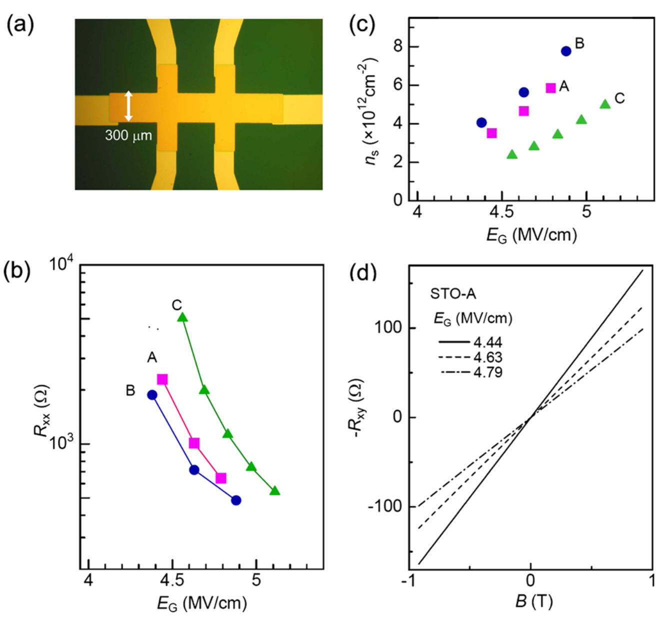

FIG. 1 (color online). (a) Photograph of a $SrTiO_3$ FET. Carriers are accumulated beneath the Hall-bar shaped gate electrode (Au). The Parylene gate insulator is homogeneously deposited within the view of this photograph and cannot be seen. (b) Sheet resistivity as a function of E_G at 2 K. (c) Hall carrier density vs E_G at 2 K showing the monotonic increase of n_s with E_G. (d) The Hall resistance -R_{xy} vs B for STO-A at 2 K.

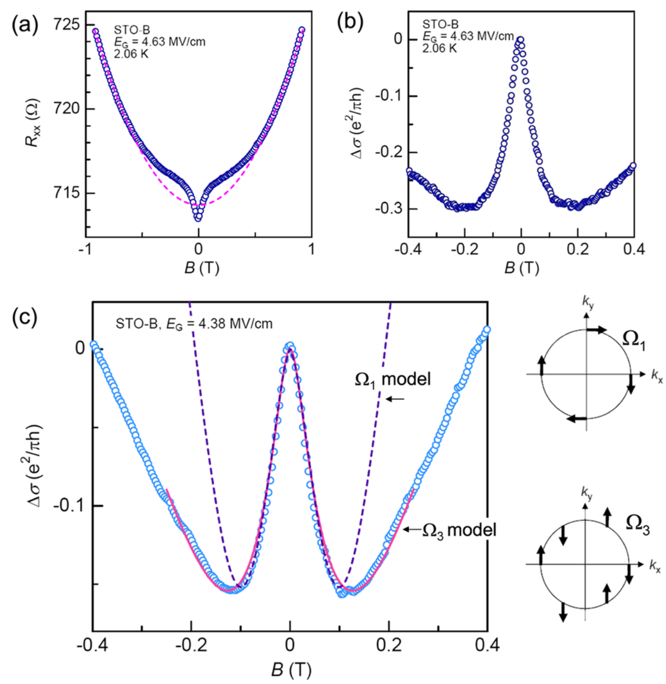

FIG. 2 (color online). (a) Magnetoresistance data (open circles) of STO-B at $E_G = 4.63$ MV/cm and the fit to B^2 background (dashed line). (b) Conductance correction $\Delta\sigma$ in unit of $e^2/\pi h$ (e is the unit charge and h is the Planck's constant) due to weak antilocalization derived by subtracting the B^2 background. (c) Theoretical fits given by the $\mathbf{\Omega}_1$-only and the $\mathbf{\Omega}_3$-only conditions (dashed and solid curves, respectively) within the ILP theory [32] to the experimental data $\Delta\sigma$ (open circles) of STO-B at $E_G = 4.38$ MV/cm. Simplified diagrams of $\mathbf{\Omega}_1$ and $\mathbf{\Omega}_3$ are also shown. The $\mathbf{\Omega}_3$ model perfectly reproduces $\Delta\sigma$.

TABLE I. Parameters used for the k-cubic ILP fitting ($B_{\mathrm{SO1}} = 0$).

	STO-A			STO-B			STO-C				
E_G(MV/cm)	4.44	4.63	4.79	4.38	4.63	4.88	4.56	4.69	4.83	4.97	5.11
B_ϕ(mT)	13.6	11.4	10.1	13.0	10.0	10.1	19.0	14.7	10.2	10.0	8.02
B_{SO3}(mT)	21	26	31	34	44	49	22	24	24	26	9

in the present system). In Fig. 2(c), we compare an experimental MR curve with models which assume either $\mathbf{\Omega}_1$-only ($m_j = \pm 1/2$) or the $\mathbf{\Omega}_3$-only ($m_j = \pm 3/2$) condition. Each model was obtained by excluding the irrelevant terms from the general expression [Eq. (13) of Ref. [32]] [34]. In this condition, the fitting parameters are characteristic magnetic fields for the phase coherence $B_\phi = \hbar/4eD\tau_\phi$ and the spin-orbit coupling $B_{\mathrm{SOn}} = \frac{\hbar}{4eD} 2\Omega_n^2 \tau_n$, where the index n takes 1 or 3, D is the diffusion constant, Ω_n is $|\mathbf{\Omega}_n|$, τ_n is the scattering time defined as $1/\tau_n = \int(1 - \cos n\varphi) W(\varphi) d\varphi$, and $W(\phi)$ is the probability of scattering by an angle φ. It is noted that τ_1 is identically equal to τ_{tr}. In what follows, the condition for an isotropic scattering ($\tau_3 = \tau_1$) is used for simplicity [36]. As can be seen from Fig. 2(c), the $\mathbf{\Omega}_3$-only model reproduces the experimental data almost perfectly, whereas they deviate from the $\mathbf{\Omega}_1$-only model especially around the minimum in the $\Delta\sigma$-B plot. On the other hand, both models give good fits for the low-B part of the magnetoconductance, because the sharpness of the fitting curves around $B = 0$ is determined mainly by B_ϕ [37]. These observations demonstrate that the k-linear model is not applicable, but the k-cubic-Rashba model is perfectly consistent with the experimental magnetoconductance. The dominance of the cubic-Rashba term is most strictly confirmed for $n_s = 2.4$–4.7×10^{12} cm^{-2}. The relatively large B_{tr} in this n_s range enabled the fitting of the $\Delta\sigma$-B plot to larger magnetic fields, which allowed us to clearly distinguish the outcomes between the linear and the cubic model fittings. The values of B_ϕ and B_{SO3} used for the k-cubic fitting are summarized in Table I.

Recent studies on the interface electron gas in $SrTiO_3$ have suggested that there exists more than one type of carrier [20,21,38]. The background MR proportional to B^2 in our system may also originate from two carriers with different mobilities, though the nonlinearity in the Hall effect that is expected in such a condition is extremely small in the present case. In terms of localization, if those carriers with different k and τ_{tr} both contribute to the localization significantly, more complicated magnetoconductance $\Delta\sigma$ should be observed [39]. The absence of such an effect in our system suggests that only one type of carrier contributes dominantly to $\Delta\sigma$. We assign the high-mobility carriers at the bottom of the conduction band, which are more strongly confined at the interface, as the source of $\Delta\sigma$. This assignment is consistent with recent studies, where the carrier effective mass is small (large) in the in-plane (out-of-plane) direction for the lowest band confined in $SrTiO_3$ [20,21]. A schematic band diagram incorporating spin splittings is shown in Fig. 4(b).

Carrier density dependence of spin-precession length (L_{SO}) and phase coherence length (L_ϕ) obtained by fitting to the $\mathbf{\Omega}_3$-only model is shown in Fig. 3(d). The relationship $B = \hbar/4eL^2$ was used to derive the length scales from the characteristic magnetic fields. L_{SO} monotonically decreases with increasing n_s (or E_G), and ranges from 88 to 58 nm. L_ϕ increases monotonically with n_s (93–140 nm). These trends are qualitatively similar to those recently reported in $KTaO_3$-FETs, although L_{SO} in $SrTiO_3$ is notably longer than that in $KTaO_3$ [40]. The shorter L_{SO} probably reflects the stronger atomic spin-orbit coupling in $KTaO_3$.

To further confirm that the k-dependent spin splitting is actually happening, we clarify the spin-precession mechanism as follows. When k-dependent band splitting

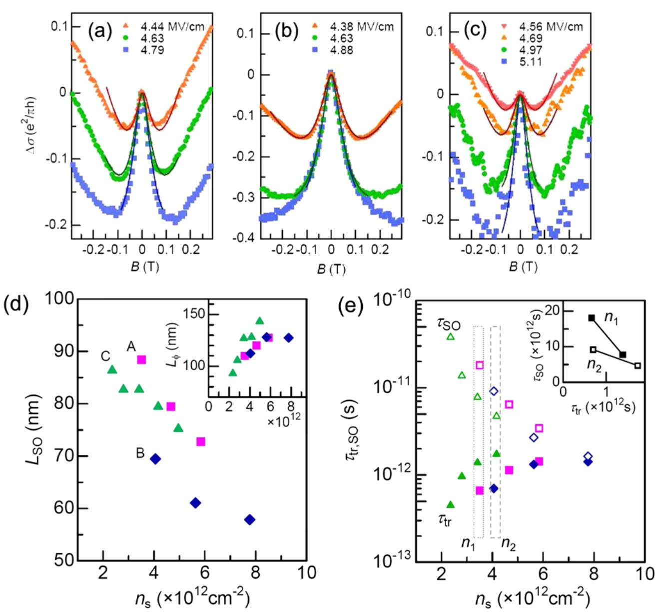

FIG. 3 (color online). Experimental $\Delta\sigma$ (closed symbols) and theoretical fit by the $\mathbf{\Omega}_3$-only condition in the ILP theory (solid curves) for (a) STO-A, (b) -B, and (c) -C, respectively. (d) Spin-precession length vs sheet carrier density n_s. The inset shows the phase coherence length vs n_s. (e) Spin-precession time (open symbols) and momentum scattering time (closed symbols) as a function of n_s. The inset shows τ_{SO} vs τ_{tr} for nearly constant n_s ($n_1 \sim 3.5 \times 10^{12}$ and $n_2 \sim 4.1 \times 10^{12}$ cm^{-2}), ruling out the Elliot-Yafet mechanism for both conditions (see text).

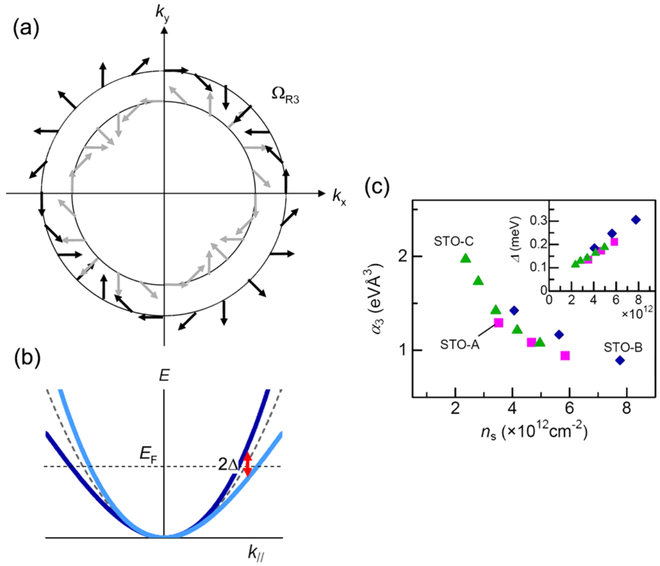

FIG. 4 (color online). (a) Schematic spin configuration for the cubic-Rashba effect [Eq. (2)]. The spin quantization axis rotates 3θ as $\mathbf{k}$ rotates θ around the Fermi circles, in contrast to the linear Rashba effect. (b) Energy diagram of the conduction band (CB) bottom of gated-$SrTiO_3$ as a function of an in-plane wave vector ($k_{\parallel}$). The band with a small effective mass forms two spin-split bands (light and dark blue curves) with energies $E = \hbar^2 k^2/2m^* \pm \alpha_3 k^3$. The approximate position of the Fermi level E_F is shown by a dashed horizontal line. (c) Deduced values for the coefficient α_3 for the cubic-Rashba effect as a function of n_s. The inset shows spin splitting energy Δ as a function of n_s. 2Δ corresponds to the difference in the energy of the two spin-split bands at E_F.

is present, spin relaxation is described by the Dyakonov-Perel mechanism, with $\tau_{SO} \propto \Delta^2/\tau_{tr}$ [41], where Δ is the spin splitting energy. On the other hand, if the spin relaxation is brought about by spin-flip scattering, i.e., the Elliot-Yafet mechanism, $\tau_{SO} \propto \tau_{tr}/n_s^2$ is the relevant result for a degenerate system [41]. Although it is not straightforward to unambiguously confirm the Dyakonov-Perel mechanism in our system, the Elliot-Yafet mechanism can be excluded as we describe below. Figure 3(e) gives τ_{SO} and τ_{tr} plotted against n_s; τ_{tr} is estimated from the measured Hall mobility assuming $m^* = 1.5$ [42], whereas τ_{SO} was derived using relations $L_{SO} = \sqrt{D\tau_{SO}}$, $D = \frac{1}{2}v_F^2\tau_{tr}$, $v_F = \hbar k_F/m^*$, and $k_F = \sqrt{2\pi n_s}$, where v_F is the Fermi velocity and k_F is the Fermi wave vector. In the inset of Fig. 3(e), we extract the relation between τ_{SO} and τ_{tr} at nearly constant values of n_s ($n_1 \sim 3.5 \times 10^{12}$ and $n_2 \sim 4.1 \times 10^{12}$ cm^{-2}) using data points from different devices. Although at constant n_s the relation $\tau_{SO} \propto \tau_{tr}$ is expected for the Elliot-Yafet mechanism, τ_{SO} decreases with increasing τ_{tr} [inset of Fig. 3(e)], ruling out the Elliot-Yafet mechanism.

Taking into account the bulk inversion symmetry of $SrTiO_3$ [17], the consistency between the experiment and the $\mathbf{\Omega}_3$-only condition of the ILP theory suggests the occurrence of the cubic-Rashba effect. We show the spin splitting energy Δ estimated from $\Delta = \hbar|\Omega_3|$ in the inset of Fig. 4(c). The spin splitting energy is 0.1–0.3 meV. To obtain the coefficient for the cubic-Rashba effect, we assumed the relation $\hbar|\Omega_3| = \alpha_3 k^3$ [2,8,23]. The value of α_3 thus calculated is shown in Fig. 4(c). We find a systematic trend in α_3 in relation to n_s.

In the light of the present finding, it would be interesting to study other spin related phenomena, such as the spin Hall effect [43,44], in $SrTiO_3$. Notably, an enhancement of the spin Hall conductivity for the cubic-Rashba Hamiltonian has been predicted [24]. On the other hand, the intrinsic spin Hall effect originally derived for a bulk GaAs hole system [43] is based on a magnetic-field-like gauge curvature, defined in a momentum space, which radiates from the Γ point (where $m_j = \pm 3/2$ and $\pm 1/2$ bands are degenerate) and shifts the motion of carriers from an electric field direction. In gated $SrTiO_3$, the degeneracy at the Γ point is removed but other singular points, i.e., the crossing of $m_j = \pm 3/2$ and $\pm 1/2$ bands, can occur. Precise tuning of the Fermi energy to such points may raise intriguing possibility for the spin Hall physics.

In conclusion, we have investigated a spin-orbit coupling in gated $SrTiO_3$, in which inversion symmetry is preserved in its bulk form. By analyzing an antilocalization effect in magnetoresistance, we observed the distinct configuration of a spin-precession vector in a k plane based on the k-cubic-Rashba effect compared to the linear Rashba effect. The unique configuration of spin-precession vector as well as the absence of the Dresselhaus term in $SrTiO_3$ may be valuable in designing future spin devices.

[1] Y. A. Bychkov and E. I. Rashba, J. Phys. C **17**, 6039 (1984).
[2] R. Winkler, *Spin-orbit Coupling Effects in Two-Dimensional Electron and Hole Systems* (Springer, Berlin, 2003).
[3] S. D. Ganichev *et al.*, Phys. Rev. Lett. **92**, 256601 (2004).
[4] L. Meier, G. Salis, I. Shorubalko, E. Gini, S. Schön, and K. Ensslin, Nature Phys. **3**, 650 (2007).
[5] W. Knap *et al.*, Phys. Rev. B **53**, 3912 (1996).
[6] T. Koga, J. Nitta, T. Akazaki, and H. Takayanagi, Phys. Rev. Lett. **89**, 046801 (2002).
[7] J. B. Miller, D. M. Zumbühl, C. M. Marcus, Y. B. Lyanda-Geller, D. Goldhaber-Gordon, K. Campman, and A. C. Gossard, Phys. Rev. Lett. **90**, 076807 (2003).
[8] R. Winkler, Phys. Rev. B **62**, 4245 (2000).
[9] G. M. Minkov, A. A. Sherstobitov, A. V. Germanenko, O. E. Rut, V. A. Larionova, and B. N. Zvonkov, Phys. Rev. B **71**, 165312 (2005).
[10] S. Faniel, T. Matsuura, S. Mineshige, Y. Sekine, and T. Koga, Phys. Rev. B **83**, 115309 (2011).
[11] J. Nitta, T. Akazaki, H. Takayanagi, and T. Enoki, Phys. Rev. Lett. **78**, 1335 (1997).
[12] J. D. Koralek, C. P. Weber, J. Orenstein, B. A. Bernevig, S.-C, Zhang, S. Mack, and D. D. Awschalom, Nature (London) **458**, 610 (2009).

[13] A. Ohtomo and H. Y. Hwang, Nature (London) **427**, 423 (2004).
[14] N. Reyren *et al.*, Science **317**, 1196 (2007).
[15] A. Brinkman, M. Huijben, M. van Zalk, J. Huijben, U. Zeitler, J. C. Maan, W. G. van der Wiel, G. Rijnders, D. H. A. Blank, and H. Hilgenkamp, Nature Mater. **6**, 493 (2007).
[16] K. Ueno, S. Nakamura, H. Shimotani, A. Ohtomo, N. Kimura, T. Nojima, H. Aoki, Y. Iwasa, and M. Kawasaki, Nature Mater. **7**, 855 (2008).
[17] L. F. Matthheis, Phys. Rev. B **6**, 4718 (1972).
[18] R. Bistritzer, G. Khalsa, and A. H. MacDonald, Phys. Rev. B **83**, 115114 (2011).
[19] H. Uwe, T. Sakudo, and H. Yamaguchi, Jpn. J. Appl. Phys. **24**, Suppl. 24-2, 519 (1985).
[20] Z. S. Popovic, S. Satpathy, and R. M. Martin, Phys. Rev. Lett. **101**, 256801 (2008).
[21] A. F. Santander-Syro *et al.*, Nature (London) **469**, 189 (2011).
[22] On the other hand, the xy state (corresponds to z-like state in p orbital) has no coupling coefficients to $m_j = \pm 1/2$ states [M. S. Dresselhaus *et al.*, *Group Theory* (Springer, Berlin, 2008), p. 525, Table D.6].
[23] L. G. Gerchikov and A. V. Subashiev, Sov. Phys. Semicond. **26**, 73 (1992).
[24] J. Schliemann and D. Loss, Phys. Rev. B **71**, 085308 (2005).
[25] M. Ben Shalom, M. Sachs, D. Rakhmilevitch, A. Palevski, and Y. Dagan, Phys. Rev. Lett. **104**, 126802 (2010).
[26] A. D. Caviglia, M. Gabay, S. Gariglio, N. Reyren, C. Cancellieri, and J.-M. Triscone, Phys. Rev. Lett. **104**, 126803 (2010).
[27] S. Maekawa and H. Fukuyama, J. Phys. Soc. Jpn. **50**, 2516 (1981).
[28] S. Hikami, A. I. Larkin, and Y. Nagaoka, Prog. Theor. Phys. **63**, 707 (1980).
[29] We neglect the effect of Zeeman splitting considered in Ref. [26].
[30] H. Nakamura, H. Takagi, I. H. Inoue, Y. Takahashi, T. Hasegawa, and Y. Tokura, Appl. Phys. Lett. **89**, 133504 (2006).
[31] D. Sekiya, H. Nakamura, and T. Kimura, Appl. Phys. Express **4**, 064103 (2011).
[32] S. V. Iordanskii, Y. B. Lyanda-Geller, and G. E. Pikus, JETP Lett. **60**, 206 (1994).
[33] In the original ILP theory [32], the cubic term due to the Dresselhaus effect is assumed. Here, we deliberately changed the notation to represent the cubic-Rashba effect because only the difference in angular harmonics is important in the ILP theory.
[34] Believing that our samples are a single-band material ($m_j = \pm 1/2$ OR $\pm 3/2$) and free from spin-flip scatterings such as Elliot-Yafet mechanism, the condition that both $\mathbf{\Omega}_1$ and $\mathbf{\Omega}_3$ coexist does not make much sense. However, to make our argument more concrete and show that the $\mathbf{\Omega}_3$-only model is indeed exclusively applicable to our experiment, we performed a series of fittings varying the values (or ratio) of $\mathbf{\Omega}_1$ and $\mathbf{\Omega}_3$. See Supplemental Material [35].
[35] See Supplemental Material at http://link.aps.org/supplemental/10.1103/PhysRevLett.108.206601 for the detail of fittings.
[36] We do not pursue the rigorousness of this assumption here, since (1) an exact form of $W(\phi)$ is unknown, (2) τ_1 nevertheless gives a good qualitative measure for the value of τ_3, and (3) our final conclusion regarding the occurrence of the k-cubic-Rashba effect on the surface of $SrTiO_3$ is unaffected by the value of τ_3.
[37] S. A. Studenikin, P. T. Coleridge, N. Ahmed, P. J. Poole, and A. Sachrajda, Phys. Rev. B **68**, 035317 (2003).
[38] T. Fix, F. Schoofs, J. L. MacManus-Driscoll, and M. G. Blamire, Phys. Rev. Lett. **103**, 166802 (2009).
[39] D. A. Dikin, M. Mehta, C. W. Bark, C. M. Folkman, C. B. Eom, and V. Chandrasekhar, Phys. Rev. Lett. **107**, 056802 (2011).
[40] H. Nakamura and T. Kimura, Phys. Rev. B **80**, 121308(R) (2009).
[41] I. Zutic, J. Fabian, and S. D. Sarma, Rev. Mod. Phys. **76**, 323 (2004).
[42] A. D. Caviglia, S. Gariglio, C. Cancellieri, B. Sacépé, A. Fête, N. Reyren, M. Gabay, A. F. Morpurgo, and J.-M. Triscone, Phys. Rev. Lett. **105**, 236802 (2010).
[43] S. Murakami, N. Nagaosa, and S. C. Zhang, Science **301**, 1348 (2003).
[44] J. Sinova, D. Culcer, Q. Niu, N. A. Sinitsyn, T. Jungwirth, and A. H. MacDonald, Phys. Rev. Lett. **92**, 126603 (2004).